Structural Characterization of Q10-Loaded Solid Lipid Nanoparticles by NMR spectroscopy

Sylvia A. Wissing,[1] Rainer H. Müller,[1] Lars Manthei,[2] and Christian Mayer[2,3]

Received September 24, 2003; accepted November 10, 2003

Purpose. The structure of loaded solid lipid nanoparticles (SLN) has been studied to elucidate the incorporation of coenzyme Q10.
Methods. Solid-state nuclear magnetic resonance (NMR) has been applied as the principal analytical approach. In order to characterize the integration of the active ingredient coenzyme Q10 inside the solid lipid matrix, measurements of the spin-lattice relaxation time in the rotating frame have been performed.
Results. A pattern of spin diffusion between protons of the lipid and protons of the coenzyme Q10 has been observed, which indicates two different fractions of the active ingredient: whereas the majority (60%) of the coenzyme Q10 is found to be homogeneously mixed with the solid lipid, the residual amount of 40% clearly forms a separate, solid phase associated to the particles.
Conclusions. A large portion of the active ingredient has been integrated homogeneously. Another, smaller fraction forms separate domains on the nanometer scale.

KEY WORDS: nuclear magnetic resonance; solid lipid nanoparticles; spin diffusion; spin-lattice relaxation in the rotating frame ($T_{1\rho}$).

INTRODUCTION

Solid lipid nanoparticles (SLN) have been developed as an alternative carrier system to liposomes or polymer nanoparticles (1). The intention was to overcome existing limitations such as poor physical stability of the particle dispersions, limited loading capacity, lack of up-scaling, and regulatory hurdles due to unaccepted excipients.

In numerous publications, SLN have been characterized regarding their physical stability, their suitability for lyophilization and spray-drying, and their structure (2–6). It has been shown that SLN are capable of protecting chemically labile drugs from degradation and also offer prolonged or sustained release (7–10). For this, various drugs or cosmetic active ingredients have been incorporated into SLN, and their release has been studied *in vitro* and *in vivo* (11–13). Furthermore, the suitability of SLN for different application routes such as parenteral, oral, dermal, and intraperitoneal application has been investigated and reviewed (14–17). For detailed information, the reader is referred to general review articles about SLN (18–20).

The analysis of the internal structure of nanoparticles still represents an interesting challenge. Among the methods commonly applied to elucidate the structural details of these systems are X-ray diffraction, differential scanning calorimetry (DSC), and nuclear magnetic resonance (NMR). Jenning *et al.* have shown in WAXS experiments that cetyl palmitate SLN provide excellent physical stability though lack sufficient drug encapsulation in the solidified state due to their highly ordered crystal structure (21). Further crystallographic SAXS and X-ray diffraction investigations on the structure of cetyl palmitate SLN have been performed by Lukowski *et al.* (22). It was found that cetyl palmitate SLN have orthorhombic lattices in contrast to the monoclinic structure reported previously.

NMR investigations have especially turned out to be a promising approach giving further insight into the structure. While high-resolution techniques prove to be a valuable source of information for all mobile or dissolved constituents in such systems (23–31), solid-state NMR is perfectly suitable to characterize the solid particles themselves (31–34). Solid-state NMR, static or in connection with magic angle spinning, can be used to characterize the molecular mobility as well as the rotational diffusion of the particles (31,32), surface exchange phenomena (30), or phase transitions of the particle matrix (33).

In order to clarify further particle homogeneity, a specific approach is introduced that is common practice for miscibility studies on polymer systems (35). It is based on measurements of the spin-lattice relaxation time in the rotating frame on proton spins, $T_{1\rho H}$. The observation of spin diffusion phenomena by determination of $T_{1\rho H}$ allows for the discrimination between homogeneously mixed phases and heterogeneous systems with domain sizes exceeding 5 nm (35). In case of a homogeneous mixture between two components A and B, both corresponding relaxation times $T_{1\rho H}$(A) and $T_{1\rho H}$(B) will necessarily be equal. In case of a heterogeneous system with components A and B forming two different phases, $T_{1\rho H}$(A) and $T_{1\rho H}$(B) generally differ as long as the domain sizes exceed approximately 5 nm. In consequence, this simple method helps to differentiate between structural alternatives such as core-shell structures or homogeneous blends.

In the following, we describe an application of this method to solid lipid nanoparticles based on cetyl palmitate and which are loaded with coenzyme Q10 as an active ingredient. The intention of the study is to differentiate clearly between two alternative structures: 1) the active ingredient forms a separate phase inside or outside the particles, or 2) the active ingredient is homogeneously blended into the solid lipid matrix. The existence of these structural models has been suggested from release experiments by Mehnert *et al.* (8,10) and should be verified in this study. Furthermore, the study was meant to elucidate if any fraction of the lipid or the active ingredient occurs in an encapsulated liquid phase inside the nanoparticles.

MATERIALS AND METHODS

Production of SLN

SLN have been prepared according to the hot-temperature high-pressure homogenization technique described in detail by Müller and Lucks (1). Briefly, the lipid

[1] Institut für Pharmazie, Freie Universität Berlin, 12169 Berlin, Germany.
[2] Institut für Chemie, Universität Duisburg-Essen, 47048 Duisburg, Germany.
[3] To whom correspondence should be addressed. (e-mail: hi408ma@uni-duisburg.de)

0724-8741/04/0300-0400/0 © 2004 Plenum Publishing Corporation

phase and the aqueous phase are heated separately and combined at elevated temperature. A pre-emulsion is formed by high-speed stirring followed by high-pressure homogenization. Upon cooling, the nanoemulsion droplets recrystallize leading to SLN. The formulations consisted of 15.2% cetyl palmitate (Cutina CP, Henkel, Germany), 4.8% coenzyme Q10 (Beiersdorf, Germany), 1.8% Tego Care 450 (Goldschmidt, Germany), and 78.2% doubly distilled water. Three homogenization cycles were performed at 85°C and applying a pressure of 500 bar using a Micron Lab 40 homogenizer (APV Systems, Unna, Germany). The samples were stored at room temperature.

Particle Size Analysis of SLN Dispersions

Particle size of the SLN dispersions was analyzed using laser diffractometry (LD) (LS230, Coulter Electronics, Krefeld, Germany) and photon correlation spectroscopy (PCS) (Zetasizer 4, Malvern Instruments, Herrenberg, Germany).

Evaluation of the LD data was performed using the Mie theory, which is applicable for particle sizes in the submicrometer range. Calculations were based on the refractive index of the dispersion medium water (1.33) and on the lipid particles (real part, 1.456; imaginary part, 0.01). The characteristic parameters d50%, d90%, d95%, and d99% are given in Table I.

For PCS measurements, the samples were diluted with bidistilled water to an appropriate count rate in order to eliminate multiple scattering. The total measurement time was 200 s (10 sample times of 20 s). The samples were measured at an angle of 90°. The average diameter was calculated according to Stokes–Einstein after a curve fitting of the correlation function was done. The average diameter (z-average) and the polydispersity index (PI) are also given in Table I.

Thermal Analysis of SLN Dispersions

Differential scanning calorimetry (DSC, DSC 821e, Mettler Toledo, Walldorf, Germany) was used to prove the solid state of the investigated SLN dispersions. The samples were heated from 25 to 85°C and subsequently cooled to 5°C at a rate of 5°C/min while flushing with nitrogen (80 ml/min). The melting and crystallization enthalpies were calculated by integration of the peak areas (Star Software, Mettler Toledo) and are listed in Table II.

Sample Preparation for NMR Measurements

In order to concentrate the samples and to remove the influence of the water, the particle suspension has been dried in a slow and careful process. For this purpose, the aqueous particle suspension was filled into a Petri dish that was stored in an exsiccator in presence of water absorbant at full atmospheric pressure. This drying process was extended until the weight of the remaining mass was constant, which generally took several days. At this point, the creamy material was carefully transferred into a cylindrical NMR sample container suitable for high-frequency sample spinning.

Solid-State Proton NMR and Relaxation Measurements

All spectra were obtained on a 400-MHz spectrometer (ASX-400, Bruker, Karlsruhe, Germany) under sample spinning at the magic angle (54.7°) and 10 kHz spinning rate. Generally, a double-frequency 4-mm MAS probe was used under constant temperature control. The free induction decay following a single 90° pulse was accumulated over 16 to 32 experiments and Fourier transformed to yield simple line spectra.

The proton spin-lattice relaxation times in the rotating frame $T_{1\rho H}$ have been measured by application of the pulse sequence shown in Fig. 1: a single 90° pulse on the proton channel is followed by a spin-lock pulse of a duration τ which is meant to keep the magnetization locked in a given orientation of the rotating frame. The relaxation of the magnetization component along this given direction is monitored at the end of the period τ by Fourier transformation of the following free induction decay. Again, 32 scans have been accumulated for each experiment at a given spin-lock time. For an analysis of the relaxation behavior, the normalized amplitudes of individual signals of the line spectra are plotted logarithmically vs. the duration of the spin-lock pulse τ.

RESULTS

The particle size of the investigated SLN formulation was completely in the nanometer range (Table I). The low polydispersity index of 0.122 indicates a narrow size distribution. Therefore, particle growth due to Ostwald ripening is not likely. Excellent long-term stability (up to 3 years) with reproducible particle sizes of this formulation has been described before (36).

It has previously been shown that bulk lipids have the tendency to recrystallize at lower temperatures (37). This melting point depression depends strongly on the particle size and can be described by the modified Thomson equation. Melting point depressions of 20°C and more have been described for lipids formulated as SLN. Therefore, standard DSC measurements are regularly performed in order to ensure and quantify the crystalline status of the SLN. If upon heating no melting peak is detectable, the formation of supercooled melts is highly likely. This has been shown for lipids such as trilaurin and trimyristin (38). Cetyl palmitate, how-

Table I. Particle Size Data (LD and PCS) of the Investigated SLN Formulation on Day 1 After Production

LD parameters [μm]				PCS parameters	
d50%	d90%	d95%	d99%	z-ave (nm)	PI
0.21 ± 0.03	0.38 ± 0.01	0.42 ± 0.01	0.49 ± 0.01	249 ± 5	0.12 ± 0.01

Characteristic LD parameters are d50%, d90%, d95%, d99%; characteristic PCS parameters are mean diameter (z-ave) and polydispersity index (PI) (n = 3).
LD, laser diffractometry; PCS, proton correlation spectroscopy; SLN, solid lipid nanoparticles.

Table II. Thermal Analysis Data of the Investigated SLN Formulation on Day 1 After Production

Heating			Cooling		
Peak onset	Peak maximum	Int. normalis.	Peak onset	Peak maximum	Int. normalis.
45.7°C	49.0°C	26.8 J/g	25.5°C	19.6°C	–26.6 J/g

The samples were heated from 25 to 85°C (heating) and subsequently cooled to 5°C (cooling) at a rate of 5°C/min while flushing with nitrogen (80 ml/min). Characteristic parameters are peak onset, peak maximum, and enthalpy (int. normalis.).

ever, is a pure wax for which the formation of highly crystalline SLN even upon storage at room temperature has been described before (21) and could be confirmed by the data shown in Table II.

Figure 2 shows a comparison of proton line spectra of the loaded solid lipid nanoparticles at 273 K (top) with corresponding spectra of the solid lipid cetyl palmitate (below) and the solid active ingredient Q10 (bottom). Clearly, the spectrum of the loaded particles represents a superposition of the spectra assigned to the two main ingredients. The particle spectrum lacks any traces of narrow resonance lines, which would indicate the presence of fluid components. Both spectra of the individual ingredients essentially consist of two peaks that can be located at approximately 1 ppm and 3.5 ppm, respectively. Whereas the spectrum of the lipid (cetyl palmitate) is almost exclusively formed by the peak at 1 ppm, the spectrum of the active ingredient Q10 consists of a large contribution of the peak at 3.5 ppm (78%) and a smaller contribution of the peak at 1 ppm (22%).

A series of spectra obtained after various spin-lock durations τ is shown in Fig. 3. They reveal a clear dependence of the line shape on the length of the spin-lock pulse: for short spin-lock durations ($\tau < 3$ ms), the relatively narrow peak at 1 ppm dominates the spectrum. After longer pulse lengths ($\tau > 8$ ms), the wide signal near 3.5 ppm clearly gains intensity and finally represents the largest share of the overall lineshape. A rough estimation for the overall value of the proton spin-lattice relaxation time in the rotating frame yields $T_{1\rho H} = 5$ ms with a slightly nonexponential behavior. Obviously, the signal relaxation of the peak at 1 ppm is more rapid than the one of the peak at 3.5 ppm.

The relaxation series is quantitatively analyzed by decomposition of the overall spectrum into a set of six Gaussian contributions A–F of various line widths. Whereas the Gaussians A, B, and C are centered at 3.5 ppm and correspond to a 78% fraction of the overall spectrum of the active ingredient, the contributions of the lipid and 22% of the Q10 are represented by the Gaussians D, E, and F centered at 1 ppm. The result of an addition of all six Gaussians shows little deviation from the experimental lineshape; an example for $\tau = 2$ ms is shown in Fig. 4. All spectra of the complete relaxation sequence (examples are shown in Fig. 3) are analyzed accordingly, using a standard least squares fit algorithm. The fact that three Gaussians are assigned to each peak accounts for more complex lineshapes of the contributions and allows for some lineshape variation during the course of the relaxation. This procedure yields two sets of corresponding amplitude contributions related to both chemical components according to

$$A_{Q10}(\tau) = (0.78)^{-1} \times [A_A(\tau) + A_B(\tau) + A_C(\tau)]$$

and

$$A_{lipid}(\tau) = [A_D(\tau) + A_E(\tau) + A_F(\tau)] - 0.22 \times A_{Q10}(\tau)$$

for each spin-lock period τ, relating to the active ingredient and the lipid, respectively.

In Fig. 5, the normalized amplitude contributions $A_{Q10}(\tau)/A_{Q10}(0)$ and $A_{lipid}(\tau)/A_{lipid}(0)$ are plotted against τ in a logarithmic scale. The resulting diagram exhibits two distinctly different sections: for short relaxation periods (0.5 ms $< \tau <$ 2 ms), the relaxation rates for the two components are obviously identical with a common relaxation time of $T_{1\rho H} = 1.9$ ms. No significant deviation between the two relaxation curves can be found within the given error margins. However, for $\tau > 2$ ms, the relaxation of the Q10 signal is

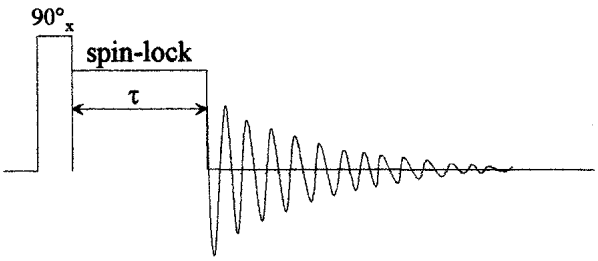

Fig. 1. Graphic representation of the pulse sequence used for measurements of proton spectra in relaxation series under variation of the spin-lock pulse duration τ.

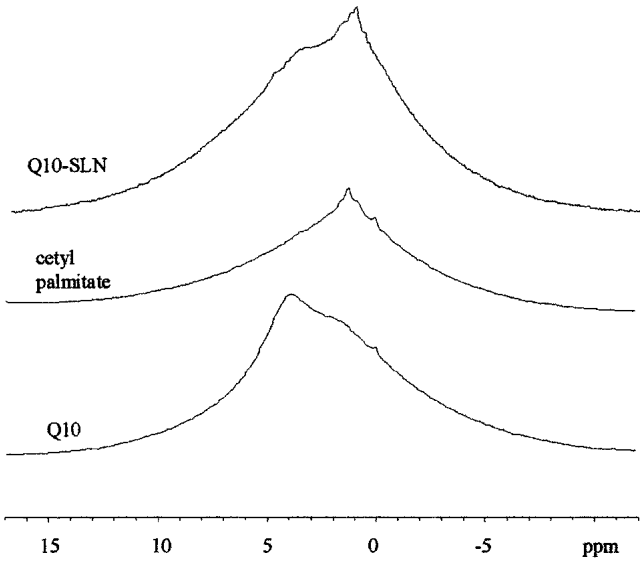

Fig. 2. Comparison of a solid-state MAS spectrum of dried, Q10-loaded SLN (top) with corresponding spectra of the solid lipid (cetyl palmitate, center) and the active ingredient Q10 (bottom).

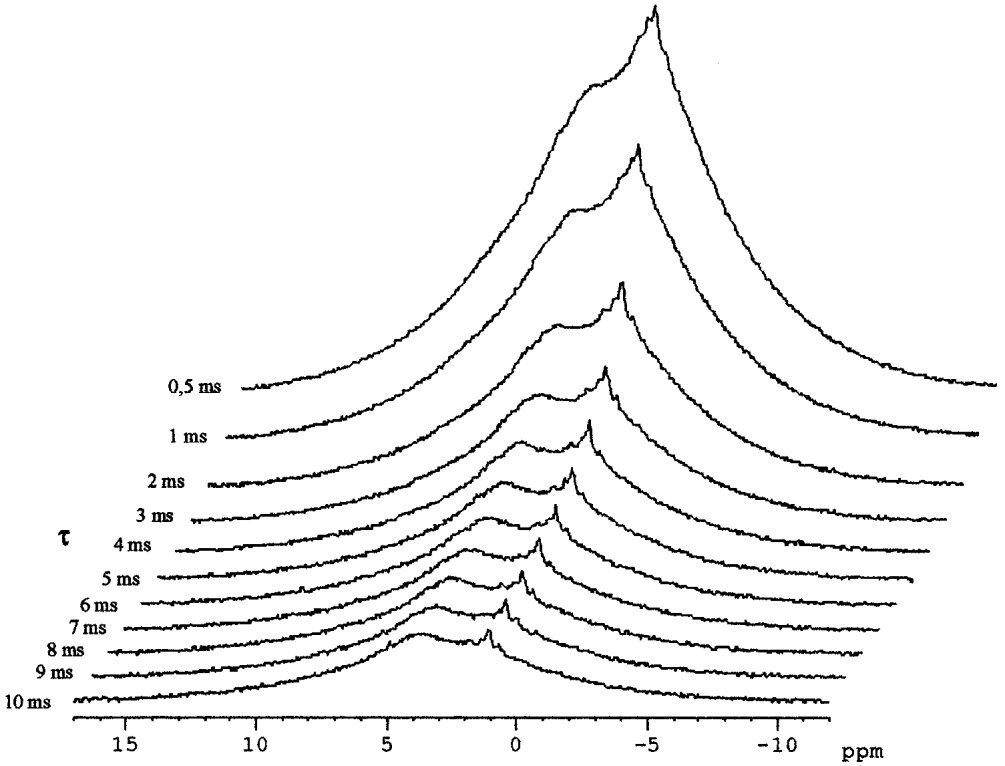

Fig. 3. Characteristic examples of MAS spectra of dried, Q10-loaded SLN obtained with the pulse sequence depicted in Fig. 1 under variation of the spin-lock pulse duration τ.

distinctly slower than the one of the lipid. In this region, the signal decay for the active ingredient Q10 is remarkably linear whereas the relaxation plot for the lipid shows some curvature and scattering. Whereas a constant relaxation time of $= 13$ ms is found for the active ingredient, the relaxation time $T_{1\rho H}$(lipid) shows a continuous increase up to approximately 5 ms. The relative contributions of the three Gaussians for each signal component (A, B, and C for the peak at 3.5 ppm and D, E, and F for the peak at 1 ppm) do not vary significantly, indicating that the individual lineshapes remain essentially unchanged during the relaxation.

The possible error in the quantitative determination of the spectral contributions $A_{Q10}(\tau)$ and $A_{lipid}(\tau)$ depends on the spectral intensity and, therefore, on the contact time τ. For $\tau < 2$ ms, we estimate an error of ± 0.1 U in $\ln[A(\tau)/A(0)]$ for both components. In case of the contribution of cetyl palmitate, the error increases to ± 0.2 U for 2 ms $< \tau <$ 5 ms. For $\tau > 5$ ms, it becomes increasingly difficult to determine the

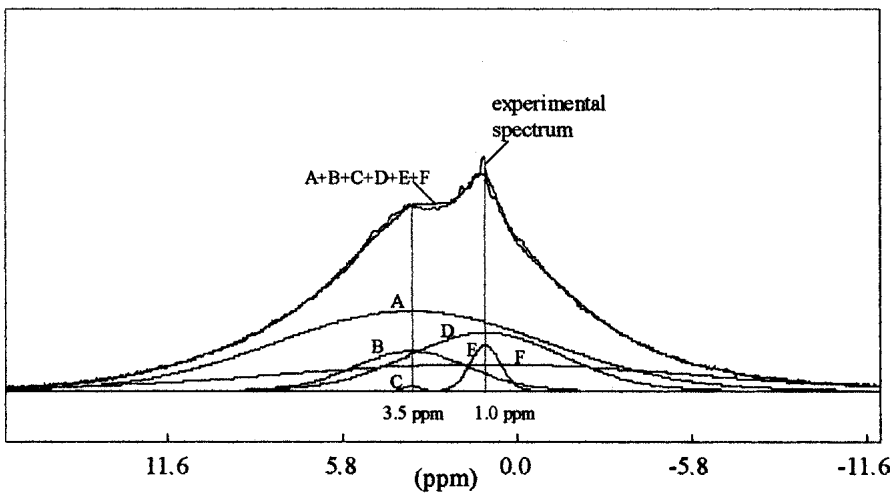

Fig. 4. Decomposition of a single spectrum of the relaxation series shown in Fig. 3 into six Gaussian contributions A–F. While the Gaussians A, B, and C are centered at 3.5 ppm and correspond to a 78% fraction of the overall spectrum of the active ingredient, the contributions of the lipid (cetyl palmitate) and 22% of the Q10 are represented by the Gaussians D, E, and F centered at 1 ppm.

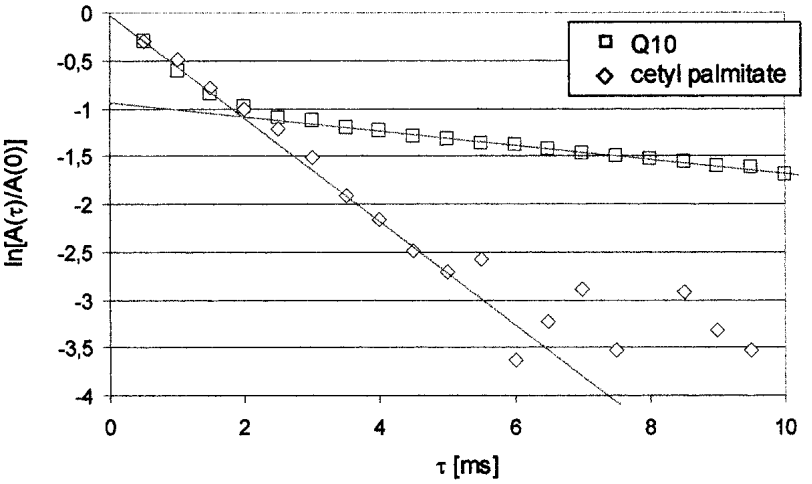

Fig. 5. Logarithmic plot of the signal contributions for Q10 (squares) and for the lipid (cetyl palmitate, diamonds) vs. the spin-lock duration τ. The gray lines indicate the linear relaxation sections with relaxation times of 1.9 ms (lipid and Q10 for $\tau < 2$ ms) and 13 ms (Q10 for $\tau > 2$ ms). The extrapolation of the latter curve toward $\tau = 0$ yields the relative amount of the 'separate' fraction of Q10 [$\exp(-0.93) \approx 0.4$].

lipid contribution against the background noise, which results in a large error margin of ±0.5 to ±1.0 U. This is also represented by a significant scattering of these values for $\tau > 5$ ms in Fig. 5. However, the error margin for the contribution of the Q10 ingredient remains at ± 0.1 U over the full range.

DISCUSSION

Based on the absence of any narrow lines in the solid-state spectra of the isolated and immobilized nanoparticles (Fig. 2, top), it can clearly be excluded that any fraction of their components larger than 0.1% forms a liquid phase. The major constituents of the solid lipid particles, the lipid itself, as well as the active ingredient Q10 occur exclusively in the solid state. They may either form a homogeneous blend or a heterogeneous mixture composed of different phases separated by a nanoscaled phase boundary.

In order to differentiate between these two structural alternatives, a series of spectral lineshapes in a $T_{1\rho H}$ relaxation experiment is analyzed for spin diffusion phenomena. In general, it is expected that different chemical components show individual $T_{1\rho H}$ relaxation curves as they differ in their intramolecular nuclear interactions as well as in their molecular mobility (35). Identical relaxation times may occur accidentally; however, this is very unlikely under the given circumstances where two compounds (Q10 and cetyl palmitate) of significantly different chemical constitution are compared. Therefore, one would expect the signals of the two components to undergo completely independent relaxation processes. On the other hand, close contact between the protons of the two molecular components may allow for a process called spin diffusion; that is, a magnetization transfer between the nuclei that leads to an efficient averaging of the spin-lattice relaxation in the rotating frame. Under these circumstances, a single decay behavior would be observed for both signals. Consequently, one may analyze the homogeneity of the mixture based on the observed relaxation plots. If the average distance between Q10 and lipid molecules exceeds 5 nm such as given for single component domains of this size range, two distinctly different relaxation times $T_{1\rho H}$(Q10) and $T_{1\rho H}$(lipid) are expected. A homogeneous mixture between Q10 and the lipid would definitely lead to a single relaxation time $T_{1\rho H}$(Q10) ≈ $T_{1\rho H}$(lipid), and a common relaxation curve would be observed due to efficient spin diffusion.

In the given case, a homogeneous mixture of the two components is indicated by the initial common signal decay observed for $0 < \tau < 2$ ms (Fig. 5). A significant portion of the active ingredient Q10 most likely forms a homogeneous mixture with the solid lipid cetyl palmitate in a single phase. However, at longer spin-lock pulse durations, it becomes obvious that another fraction of the active ingredient Q10 occurs in a separate phase independent from the solid lipid/Q10 blend. A clear-cut separation of the two branches of the Q10 relaxation curve is found, which indicates a distinct spatial separation of the two phases. An extrapolation of the second, flat part of the Q10 relaxation curve toward $\tau = 0$ yields a relative contribution of this separate fraction of Q10 of roughly 40% (±3%). Consequently, the larger fraction of 60% (±3%) of the active ingredient Q10 occurs in the homogeneous mixture with the solid lipid.

Of course, this result does not yet answer detailed questions on the microscopic structure of the heterogeneous particles in detail. With the given result of the spin diffusion behavior, the separate fraction of Q10 may form single or multiple inclusions within the solid lipid/Q10 blend. In addition, it may also appear as a single layer around a homogeneous lipid/Q10 sphere in a concentric core-shell arrangement. These alternative structures may be discriminated by additional NMR experiments using paramagnetic ions (e.g., Mn^{2+}) in the aqueous phase: in a core-shell structure, the outer phase (e.g., the "separate" Q10) should be strongly affected by the dipolar coupling with the electron spins, leading to additional line broadening and a significant decrease of relaxation times. The particle core, on the other hand, should be protected from this influence under these circumstances.

The introduction of solid-state NMR is not meant to compete with other existing techniques, but to extend the knowledge on the given systems beyond the point that is ac-

cessible by other existing methods. The main advantage of NMR vs. all other analytical approaches is its capability for an unambiguous identification of chemical compounds. In contrast to all alternatives, NMR allows for a clear molecular assignment (by chemical shifts and/or intramolecular coupling phenomena), while at the same time, crucial questions about for example, molecular mobility, intermolecular distances, or diffusion properties may be answered.

REFERENCES

1. R. H. Müller and J. S. Lucks. Arzneistoffträger aus festen Lipidteilchen, Feste Lipidnanosphären (SLN). European Patent EP 0605497 (1996).
2. R. H. Müller, A. Dingler, H. Weyhers, A. zur Mühlen, and W. Mehnert. Solid lipid nanoparticles (SLN) – ein neuartiger Wirkstoff-Carrier für Kosmetika und Pharmazeutika. III. Langzeitstabilität, Gefrier- und Sprühtrocknung. *Pharm. Ind.* **59**:614–619 (1997).
3. H. Heiati, R. Tawashi, and N. C. Phillips. Drug retention and stability of solid lipid nanoparticles containing azidothymidine palmitate after autoclaving, storage and lyophilization. *J. Microencaps.* **15**:173–184 (1998).
4. C. Freitas and R. H. Müller. Spray drying of solid lipid nanoparticles. *Eur. J. Pharm. Biopharm.* **46**:145–151 (1998).
5. E. Zimmermann, R. H. Müller, and K. Mäder. Influence of different parameters on reconstitution of lyophilized SLN. *Int. J. Pharm.* **19**:211–213 (2000).
6. A. Radomska, R. Dobrucki, and R. H. Müller. Chemical stability of the lipid matrices of solid lipid nanoparticles (SLN) – development of the analytical method and determination of long-term stability. *Pharmazie* **54**:903–909 (1999).
7. H. Heiati, R. Tawashi, R. R. Shivers, and N. C. Phillips. Solid lipid nanoparticles as drug carriers. I. Incorporation and retention of the lipophilic prodrug 3′-azido-3′-deoxythymidine palmitate. *Int. J. Pharm.* **146**:123–131 (1997).
8. W. Mehnert, A. zur Mühlen, A. Dingler, H. Weyhers, and R. H. Müller. Solid lipid nanoparticles (SLN) – ein neuartiger Wirkstoff-Carrier für Kosmetika und Pharmazeutika. II. Wirkstoff-Inkorporation, Freisetzung und Sterilisierbarkeit. *Pharm. Ind.* **59**: 511–514 (1997).
9. S. A. Wissing and R. H. Müller. Solid lipid nanoparticles as carrier for sunscreens: in vitro release and in vivo skin penetration. *J. Control. Rel.* **81**:225–233 (2002).
10. A. zur Mühlen, C. Schwarz, and W. Mehnert. Solid lipid nanoparticles (SLN) for controlled drug delivery – drug release and release mechanism. *Eur. J. Pharm. Biopharm.* **45**:149–155 (1998).
11. V. Jenning, M. Schäfer-Korting, and S. Gohla. Vitamin A loaded solid lipid nanoparticles for topical application: drug release properties. *J. Controlled Release* **66**:115–126 (2000).
12. D. B. Chen, T. Z. Yang, W. L. Lu, and Q. Zhang. In vitro and in vivo study of two types of long-circulating solid lipid nanoparticles containing paclitaxel. *Chem. Pharm. Bull.* **49**:1444–1447 (2001).
13. S. A. Wissing and R. H. Müller. The influence of solid lipid nanoparticles (SLN) on skin hydration and viscoelasticity – in vivo study. *Eur. J. Pharm. Biopharm.* **561**:67–72 (2003).
14. A. Fundaro, R. Cavalli, A. Bargoni, D. Vighetto, G. P. Zara, and M. R. Gasco. Non-stealth and stealth solid lipid nanoparticles (SLN) carrying doxorubicin: pharmacokinetics and tissue distribution after i.v. administration to rats. *Pharm. Res.* **42**:337–343 (2000).
15. S. Yang, J. Zhu, Y. Lu, B. Liang, and C. Yang. Body distribution of camptothecin solid lipid nanoparticles after oral administration. *Pharm. Res.* **16**:751–757 (1999).
16. R. H. Müller, M. Radtke, and S. A. Wissing. Solid lipid nanoparticles (SLN) and nanostructured lipid carriers (NLC) in cosmetic and dermatological preparations. *Adv. Drug Del. Rev.* **54**:S131–S155 (2002).
17. S. C. Yang, L. F. Lu, Y. Cai, J. B. Zhu, B. W. Liang, and C. Z. Yang. Body distribution in vice of intravenously injected camptothecin solid lipid nanoparticles and targeting effect on brain. *J. Control. Rel.* **59**:299–307 (1999).
18. R. H. Müller, W. Mehnert, J. S. Lucks, C. Schwarz, A. zur Mühlen, H. Weyhers, C. Freitas, and D. Rühl. Solid lipid nanoparticles (SLN)—an alternative colloidal carrier system for controlled drug delivery. *Eur. J. Pharm. Biopharm.* **41**:62–69 (1995).
19. R. H. Müller, K. Mäder, and S. Gohla. Solid lipid nanoparticles (SLN) for controlled drug delivery – a review of the state of the art. *Eur. J. Pharm. Biopharm.* **50**:161–178 (2000).
20. W. Mehnert and K. Mäder. Solid lipid nanoparticles – production characterization and applications. *Adv. Drug Del. Rev.* **47**:165–196 (2001).
21. V. Jenning and S. H. Gohla. Comparison of wax and glyceride solid lipid nanoparticles (SLN). *Int. J. Pharm.* **196**:219–222 (2000).
22. G. Lukowki, J. Kasbohm, P. Pflegel, A. Illing, and H. Wulff. Crystallographic investigation of cetyl palmitate solid lipid nanoparticles. *Int. J. Pharm.* **196**:201–205 (2000).
23. V. Jenning, K. Mäder, and S. H. Gohla. Solid lipid nanoparticles (SLN) based on binary mixtures of liquid and solid lipids: a ^{1}H-NMR study. *Int. J. Pharm.* **205**:15–21 (2000).
24. K. Westesen and T. Wehler. Physicochemical characterization of a model intravenous oil-in-water emulsion. *J. Pharm. Sci.* **81**:777–786 (1992).
25. K. Westesen and T. Wehler. Investigation of the particle size distribution of a model intravenous emulsion. *J. Pharm. Sci.* **82**: 1237–1244 (1993).
26. K. Westesen, A. Gerke, and M. H. J. Koch. Characterization of native and drug-loaded human low density lipoproteins. *J. Pharm. Sci.* **84**:139–147 (1995).
27. K. Westesen, H. Bunjes, and M. H. J. Koch. Physicochemical characterization of lipid nanoparticles and evaluation of their drug loading capacity and sustained release potential. *J. Control. Rel.* **48**:223–226 (1997).
28. E. Zimmermann, S. Liedtke, R. H. Müller, and K. Mäder. ^{1}H-NMR as a method to characterize colloidal carrier systems. *Proc. Intl. Symp. Control. Rel. Bioact. Mater.* **26**:595–596 (1999).
29. S. Liedtke, E. Zimmermann, R. H. Müller, and K. Mäder. Physical characterisation of solid lipid nanoparticles (SLN^{TM}). *Proc. Intl. Symp. Control. Rel. Bioact. Mater.* **26**:599–600 (1999).
30. D. Hoffmann and C. Mayer. Cross polarization induced by temporary adsorption: NMR investigations on nanocapsule dispersions. *J. Chem. Phys.* **112**:4242–4250 (2000).
31. C. Mayer. Nuclear magnetic resonance on dispersed nanoparticles. *Prog. Nucl. Reson. Spectrosc.* **40**:307–365 (2002).
32. C. Mayer and G. Lukowski. Solid state NMR investigations on nanosized carrier systems. *Pharm. Res.* **17**:486–489 (2000).
33. S. Guinebretiere, S. Briancon, J. Lieto, C. Mayer, and H. Fessi. Study on the emulsion-diffusion of solvent: preparation and characterization of nanocapsules. *Drug Dev. Res.* **57**:18–33 (2002).
34. C. Mayer, D. Hoffmann, and M. Wohlgemuth. Structural analysis of nanocapsules by nuclear magnetic resonance. *Int. J. Pharm.* **242**:37–46 (2002).
35. W. S. Veeman and W. E. J. R. Maas. Solid state NMR techniques for the study of polymer-polymer miscibility. In P. Diehl, E. Fluck, H. Günther, R. Kosfeld, and J. Seelig (eds.), *NMR: Basic Principles and Progress*, Springer-Verlag, Berlin, 1994, pp. 131–162.
36. A. Dingler. Feste Lipid-Nanopartikel als kolloidale Wirkstoffträgersysteme zur dermalen Applikation, Ph.D. Thesis, FU Berlin (1998).
37. H. Bunjes, M. H. J. Koch, and K. Westesen. Effect of particles size on colloidal solid triglycerides. *Langmuir* **16**:5234–5241 (2000).
38. K. Westesen and H. Bunjes. Do nanoparticles prepared from lipids solid at room temperature always possess a solid lipid matrix? *Int. J. Pharm.* **115**:129–131 (1995).